Crystal Structures of Three Misacylating Mutants of *Escherichia coli* Glutaminyl-tRNA Synthetase Complexed with $tRNA^{Gln}$ and ATP†

John G. Arnez‡ and Thomas A. Steitz*

Departments of Molecular Biophysics and Biochemistry and of Chemistry and Howard Hughes Medical Institute, Yale University, New Haven, Connecticut 06520-8114

Received June 25, 1996⊗

ABSTRACT: Three previously described mutant *Escherichia coli* glutaminyl-tRNA synthetase (GlnRS) proteins that incorrectly aminoacylate the amber suppressor derived from $tRNA^{Tyr}$ (*sup*F) with glutamine were cocrystallized with wild-type $tRNA^{Gln}$ and their structures determined. In two of the mutant enzymes studied, Asp235, which contacts base pair G3-C70 in the acceptor stem, has been changed to asparagine in GlnRS7 and to glycine in GlnRS10. These mutations result in changed interactions between Asn235 of GlnRS7 and G3-C70 of the tRNA and an altered water structure between Gly235 of GlnRS10 and base pair G3-C70. These structures suggest how the mutant enzymes can show only small changes in their ability to aminoacylate wild-type cognate tRNA on the one hand and yet show a lack of discrimination against a noncognate U3-A70 base pair on the other. In contrast, the change of Ile129 to Thr in GlnRS15 causes virtually no change in the structure of the complex, and the explanation for its ability to misacylate *sup*F is unclear.

The accuracy of protein synthesis depends on the specificity of aminoacylation of transfer RNA (tRNA),[1] a reaction catalyzed by a family of enzymes called aminoacyl-tRNA synthetases (aaRS). Although all tRNAs are structurally very similar, aaRS are highly selective for their cognate tRNAs. Each tRNA possesses certain features that enable its cognate aaRS to recognize and aminoacylate it. In addition, it harbors certain elements that cause noncognate aaRS to reject it. These two aspects combined constitute the identity elements of the tRNA (Schulman, 1991). The issue that we wish to address here is how specific mutations in glutaminyl-tRNA synthetase (GlnRS) can alter its ability to recognize one of the specific identity elements in $tRNA^{Gln}$, G3-C70.

Aminoacyl-tRNA synthetases are a diverse family of enzymes, organized into two classes of ten members each on the basis of the structural fold in their active site domains (Eriani *et al.*, 1990; Ruff *et al.*, 1991). Class I aaRS contain signature amino acid sequences KMSKS and HIGH and are exemplified by glutaminyl-tRNA synthetase (GlnRS), whose structure in complex with its cognate tRNA has been determined (Rould *et al.*, 1989, 1991). Their active site domains are based on the Rossmann fold nucleotide-binding motif, an alternating $\alpha-\beta$ structure with a central parallel β-sheet (Rossmann *et al.*, 1974). In contrast with class I enzymes, class II aaRS do not contain the Rossmann fold in their active site domains but an antiparallel β-sheet that contains three concatenated homologous sequence motifs (Eriani *et al.*, 1990; Delarue & Moras, 1993). Two of these aaRS have been analyzed in complex with their cognate tRNAs, AspRS (Ruff *et al.*, 1991) and SerRS (Biou *et al.*, 1994). These two different constructions also bind different sides of the helical acceptor arm of their cognate tRNA. GlnRS, a class I aaRS, interacts with the minor groove side (Rould *et al.*, 1989) while AspRS and SerRS, both class II enzymes, bind the major groove side (Ruff *et al.*, 1991; Biou *et al.*, 1994). Additional tRNA specificities, such as anticodon recognition, are achieved by extra polypeptide modules that are attached to the core active site domains (Jasin *et al.*, 1983; Rould *et al.*, 1989, 1991; Delarue & Moras, 1993).

The crystal structure of glutaminyl-tRNA synthetase (GlnRS) complexed with $tRNA^{Gln}$ and ATP (Rould *et al.*, 1989, 1991; Figure 1A) provides detailed information on the interactions between the synthetase and its cognate tRNA. GlnRS interacts in a base-specific manner with nucleotide residues in the acceptor stem (G2-C71, G3-C70), anticodon loop (C or U at position 34, U35, G36), and D-arm (G10-C25, C16) of $tRNA^{Gln}$ (Figure 1B). These residues of the tRNA constitute part of the recognition set for GlnRS and the identity of $tRNA^{Gln}$ (Rould *et al.*, 1989, 1991; Jahn *et al.*, 1991; Hayase *et al.*, 1992). The anticodon interacts with the C-terminal double β-barrel domain, while the acceptor stem is recognized by the active site domain. The latter consists of a Rossmann fold core with an inserted acceptor-binding subdomain and contains three structural elements that interact with the three terminal base pairs of the tRNA, two loops and an α-helix. The first loop (residues 133−140) breaks up the terminal base pair U1-A72 and thus facilitates the bending of the 3′-CCA into the active site. The second loop (residues 179−184) contacts base pair G2-C71 through direct and water-mediated hydrogen bonds by backbone atoms of the loop. The α-helix, called helix H, interacts with base pair G3-C70 through Asp235. It also extends into the active site cleft and forms part of the nucleotide-binding fold (Rould *et al.*, 1989, 1991).

† This research was supported by NIH Grant GM-22778 (to T.A.S.).

* Author to whom correspondence should be addressed.

‡ Present address: Institut de Génétique et de Biologie Moléculaire et Cellulaire, CNRS/INSERM/ULP, BP 163, 67404 Illkirch Cedex, France.

⊗ Abstract published in *Advance ACS Abstracts,* November 1, 1996.

[1] Abbreviations: tRNA, transfer ribonucleic acid; GlnRS, glutaminyl-tRNA synthetase; AspRS, aspartyl-tRNA synthetase; SerRS, seryl-tRNA synthetase; aaRS, aminoacyl-tRNA synthetase; ATP, adenosine triphosphate; rms, root mean square.

S0006-2960(96)01532-2 CCC: $12.00

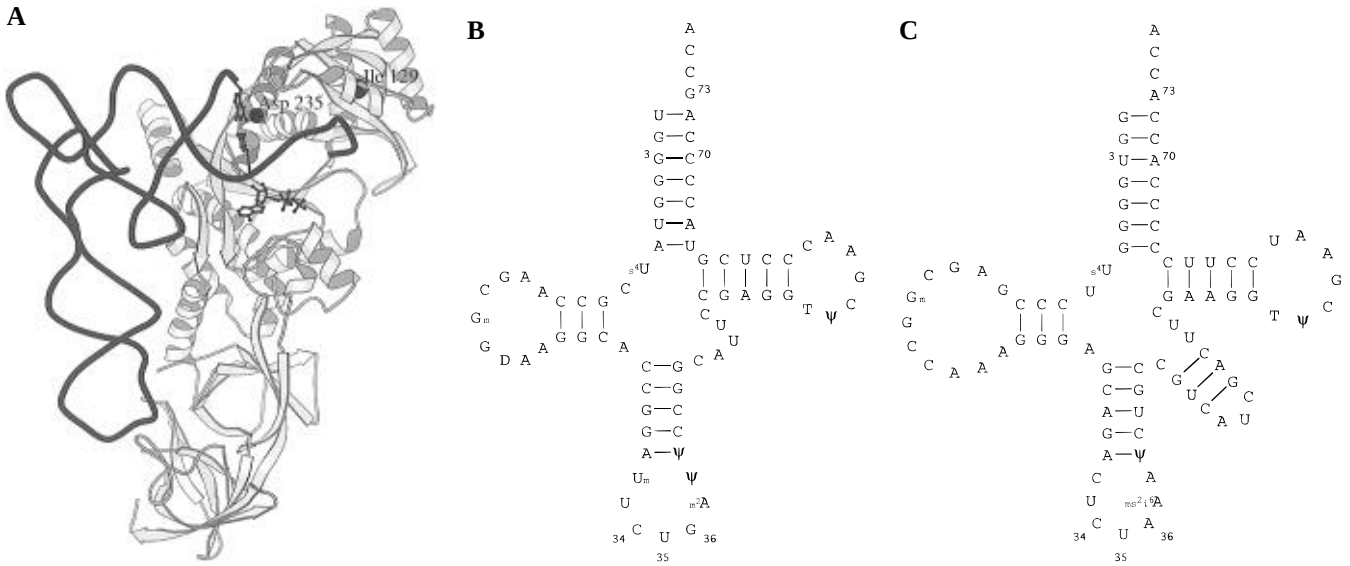

FIGURE 1: (A) Backbone drawing of the crystal structure of GlnRS complexed with $tRNA^{Gln}_2$ and ATP (Rould *et al.*, 1989). Shown also are Asp235 and Ile129, the two residues whose mutations led to mischarging phenotypes. Helix H is highlighted. Sequences of (B) $tRNA^{Gln}_2$ and (C) amber suppressor derived from $tRNA^{Tyr}$ (*sup*F) drawn in cloverleaf representation.

Three mutant GlnRS proteins having altered specificity for tRNA charging were isolated by Söll and colleagues using an *in vivo* genetic approach; strains able to misacylate with glutamine the amber suppressor derived from $tRNA^{Tyr}$ (*sup*F, Figure 1C) in order to suppress an amber mutation in the gene for β-galactosidase (*lac*Z_{1000}) were selected for their ability to grow on minimal lactose media (Inokuchi *et al.*, 1984; Swanson, 1988; Perona *et al.*, 1989). In a wild-type *gln*S background the *lac*Z_{1000} mutation can be suppressed by the amber suppressor derived from $tRNA^{Gln}$ but not by *sup*F (Uemura *et al.*, 1988). Only glutamine insertion at that position gives rise to an active β-galactosidase. Two of the mutations that confer the ability on *gln*S to misaminoacylate *sup*F were at residue 235, Asp235 to Asn (D235N, GlnRS7) and Asp235 to Gly (D235G, GlnRS10). A third mutant protein was also isolated that had a different change, Ile129 to Thr (I129T, GlnRS15). *In vivo* and *in vitro* misacylation tests have shown that GlnRS15 has the weakest mischarging activity and that GlnRS10 mischarges less efficiently than GlnRS7 (Swanson, 1988; Uemura *et al.*, 1988; Perona *et al.*, 1989). Asp235, part of helix H, contacts base pair G3-C70 in the acceptor stem of $tRNA^{Gln}$, whereas Ile129 is located in the acceptor stem binding subdomain, part of the helix leading into the loop that breaks the terminal base pair (Rould *et al.*, 1989; Figure 1A).

These mutant enzymes retain their specificity for $tRNA^{Gln}$ and do not exhibit a general broadening of specificity (Inokuchi *et al.*, 1984; Swanson, 1988). They misacylate with glutamine at low levels *in vitro* only a small set of noncognate amber suppressors. These are derived from $tRNA^{Tyr}$, $tRNA^{Trp}$ (*sup*U), $tRNA^{Glu}$, $tRNA^{fMet}$, $tRNA^{Ser}_1$, $tRNA^{Ser}_3$, and $tRNA^{Gly}$ (Hoben, 1984; Swanson, 1988). GlnRS7 is highly specific for *sup*F and *sup*U *in vivo*; other noncognate amber suppressors examined were not glutaminylated (Inokuchi *et al.*, 1984). Wild-type GlnRS, when present in high concentrations, also has the capacity to misglutaminylate the same set of noncognate tRNAs; upon overproduction in *Escherichia coli* it acylates *sup*F with glutamine. However, when the level of $tRNA^{Gln}$ is simultaneously increased, mischarging is abolished (Swanson *et al.*, 1988).

In vivo, mischarging is limited to suppressor tRNAs, while only small amounts of other tRNAs may be misacylated. For example, *sup*F is the predominant mischarged species while wild-type $tRNA^{Tyr}$ is not significantly glutaminylated (Inokuchi *et al.*, 1984). This is not surprising, as the anticodon bases interact with the protein in a highly specific manner (Rould *et al.*, 1991). The amber suppressor anticodon (CUA) is more closely related to the two glutamine-specific anticodons, CUG and UUG, than is the anticodon for tyrosine, GUA (Sprinzl *et al.*, 1987).

In order to understand the structural basis of the specificity of wild-type and mutant GlnRS enzymes for its cognate tRNA and to gain some insight into why these mutant enzymes are capable of mischarging *sup*F, we have determined the structures of these three mutant GlnRS proteins complexed with wild-type $tRNA^{Gln}$. These structures provide explanations for why mutations of Asp235 to Asn or Gly remove the enzyme's ability to discriminate between G3-C70 and U3-A70, thus eliminating base pair 3−70 as a recognition element.

MATERIALS AND METHODS

Purification of $tRNA^{Gln}$. $tRNA^{Gln}$ was overproduced by growth and induction of cells of the strain K12ΔH1Δtrp/pRS3 (Perona *et al.*, 1988) (a gift of D. Söll, Yale University, New Haven, CT) and purified as described by Perona *et al.* (1988). After fractionation over HPLC, the tRNA was desalted on a Sephadex G-25 gel filtration column (2.5 cm diameter × 16.5 cm, 81 mL), aliquoted into several tubes, lyophilized, and stored at −20 °C. An aliquot was redissolved in a small volume of distilled water prior to use in cocrystallization with mutant GlnRS proteins.

Purification of Mutant GlnRS Enzymes. Each mutant GlnRS protein was purified according to the procedure described by Hoben and Söll (1985). Cells of the *E. coli* deletion strain X3R2 (J. Plumbridge and D. Söll, unpublished results) harboring a pBR322 derivative plasmid containing a mutant *gln*S gene [pYY140 (*gln*S7) (Inokuchi *et al.*, 1984), pRS4 (*gln*S10) (Swanson, 1988), pRS12 (*gln*S15) (Swanson, 1988)] and cured of the phage λ EH4 (Swanson, 1988)

(kindly provided by D. Söll, Yale University, New Haven, CT) were grown overnight at 37 °C in LB medium supplemented with 0.5 g/L ampicillin. Twenty-four liters of culture was grown for each mutant protein, yielding approximately 100 g of cells. After phosphocellulose P-11 (Whatman) chromatography the mutant protein was better than 95% pure; an additional step, high-resolution anion-exchange chromatography [FPLC on Mono-Q (Pharmacia)] removed most of the remaining contaminants. P11 chromatography fractions containing mutant GlnRS protein were pooled and dialyzed against two changes of 2 L each of 25 mM Tris-HCl, pH 7.6, 20 mM KCl, 2 mM dithiothreitol (DTT), and 5% glycerol. They were then loaded onto a 35 mL Pharmacia FPLC Mono-Q column preequilibrated with 25 mM Tris-HCl, pH 7.6, 20 mM KCl, 2 mM DTT, 0.02% NaN_3, and 5% glycerol. The protein was eluted with a 20 mM KCl to 0.3 M KCl gradient at 5 mL/min over 80 min; GlnRS activity eluted at 140 mM KCl. Fractions containing mutant GlnRS protein were pooled and concentrated by ultrafiltration in Centriprep 30 vessels (Amicon). Silver-stained 10−15% polyacrylamide−sodium dodecyl sulfate PhastGels (Pharmacia LKB Biotech) showed few contaminants at very low levels. Purified mutant protein was dialyzed against 20 mM K_2HPO_4, pH 7.2, 50 mM KCl, 1 mM DTT, and 50% glycerol for storage at −20 °C and 10 mM PIPES, pH 7, and 1 mM DTT for crystallization. Its concentration was deduced from absorbance at 280 nm, using an extinction coefficient of 1.12 cm^{-1} mg^{-1} (Perona, 1990). Aminoacylation assays were performed according to Hoben and Söll (1985). About 20 mg of pure mutant protein was obtained per 100 g of cells.

Cocrystallization of Mutant GlnRS Enzymes with $tRNA^{Gln}$ and ATP. Each of the three mutant GlnRS proteins was complexed with $tRNA^{Gln}$ in a ratio of 1 mol of GlnRS to 1.2 mol of $tRNA^{Gln}$ such that the final concentration of the complex was 10−15 mg/mL. The resulting complex was crystallized at 17 °C using the hanging drop vapor diffusion method and conditions described by Rould *et al.* (1989) and Perona *et al.* (1988): 80 mM PIPES, pH 7−7.5, 20 mM $MgSO_4$, 0.02% NaN_3, 1.8−2.0 M $(NH_4)_2SO_4$, and 8 mM ATP. Crystals obtained were typically $0.3 \times 0.5 \times 1.5$ mm^3; they were harvested into a stabilizing solution containing 2.3 M $(NH_4)_2SO_4$, 30 mM $MgSO_4$, 80 mM NaPIPES, pH 7.0, 0.02% NaN_3, and 4 mM ATP (Rould, 1991).

Structure Determination. Mutant GlnRS enzymes complexed with $tRNA^{Gln}$ and ATP crystallized isomorphously with the wild-type complex (Rould *et al.*, 1989) in the orthorhombic space group $C222_1$ and with unit cell dimensions $a = 243.7$ Å, $b = 93.7$ Å, and $c = 115.9$ Å (GlnRS7 complex), $a = 243.5$ Å, $b = 93.7$ Å, and $c = 115.9$ Å (GlnRS10 complex), and $a = 242.0$ Å, $b = 93.7$ Å, and $c = 115.5$ Å (GlnRS15 complex).

X-ray diffraction intensities from crystals of each mutant GlnRS complexed with $tRNA^{Gln}$ and ATP were measured at 4 °C on a Xuong-Hamlin multiwire area detector using the University of California at San Diego data collection and reduction software (Howard *et al.*, 1985). Data were collected in the resolution range of 8.0−2.5 Å. Three crystals were used for each data set. Observed reflection data were processed using a procedure developed by M. Rould (SCALAR; Rould, 1991) whereby they were locally scaled to a wild-type native GlnRS−$tRNA^{Gln}$−ATP data set; at least 200 reflections were used in each local scaling neighborhood. Data collection and reduction for each of the three mutant complexes are summarized in Table 1.

Table 1: Summary of Crystallographic Data Collection[a]

	GlnRS7[b]	GlnRS10[b]	GlnRS15
resol (Å)	8.0−2.6	8.0−2.7	9.0−3.0
n. refl	36285	33823	23275
multipl	3.3	2.8	2.7
R_{merge} (%)	4.7	6.2	9.7
compl (%)	91.4	95.7	90.7
R_{cross} (%)	15	12.7	15.4

[a] resol, resolution range; n. refl, number of reflections; multipl, average multiplicity of observations per reflection; compl, completenes of data in the given resolution shell; $R_{merge} = (\sum_{hkl}|I_{i,hkl} - \langle I_{hkl}\rangle|)/\sum_{hkl}\langle I_{hkl}\rangle$, where $I_{i,hkl}$ is the ith observation of reflection hkl. $R_{cross} = (\sum_{hkl}|I_{m,hkl} - I_{n,hkl}|)/\sum_{hkl}I_{n,hkl}$, where $I_{m,hkl}$ is the mutant intensity and $I_{n,hkl}$ is the native (wild-type) intensity. [b] R_{cross} between GlnRS7 and GlnRS10 = 15%.

Difference Fourier electron density maps were calculated using F_o(mutant) − F_o(wild type) as amplitudes, calculated phases derived from the refined structure model of the wild-type complex at 4 °C (Rould *et al.*, 1989; Perona *et al.*, 1993), and the program X-PLOR (Brünger, 1990).

Refinement. Electron density maps were interpreted and structures rebuilt using the computer graphics programs FRODO (Jones, 1982) and O (Jones *et al.*, 1991). In order to obtain the starting structures for the GlnRS7 and GlnRS10 complexes, the structure of the wild-type complex at 4 °C (Rould *et al.*, 1989; Perona *et al.*, 1993) was refit in the region around residue 235 according to electron density maps calculated using $2F_o$(mutant) − F_o(wild type) as amplitudes in the Fourier synthesis. The resulting structures were refined through several cycles against appropriate data sets using X-PLOR and old protein and nucleic structure parameters (Brünger, 1990). To examine the goodness of fit, $2F_o - F_c$ maps were computed after each refinement cycle.

Subsequently, both wild-type structures, the GlnRS complex at 4 °C (Rould *et al.*, 1989) and the GlnRS complex at −20 °C (Rould *et al.*, 1991), were rerefined using new structure parameters for proteins (Engh & Huber, 1991) and nucleic acids (Parkinson *et al.*, 1996). Phases derived from the rerefined 4 °C model were then used to calculate new electron density maps using $2F_o$(mutant) − F_o(wild type) as amplitudes. The structures of the GlnRS7 and GlnRS10 complexes were then reexamined against these maps and refined using the new parameters. The solvent structure in the different complexes was checked against $F_o - F_c$ and $2F_o - F_c$ maps where the solvent had been omitted from the models, and then the models were energy minimized before calculating the phases and structure factor amplitudes.

A simulated annealing omit map was computed for each GlnRS7 and GlnRS10 complex using a procedure in X-PLOR (Brünger, 1992; Hodel *et al.*, 1992) in order to remove model bias in the region of the map in the neighborhood of residue 235. This was achieved by first omitting the residues within 14 Å of the 2-amino nitrogen of G3 in the structure of the wild-type complex [approximately the region that had undergone structural changes as indicated by the F_o(mutant) − F_o(wild type) electron density map] and then simulating heating of the molecule to 3000 K by molecular dynamics and slowly cooling it to 300 K while refining the coordinates against the diffraction data for the mutant complex. In each case, the resulting model was energy minimized and then used to generate the phases and F_cs for the map. The

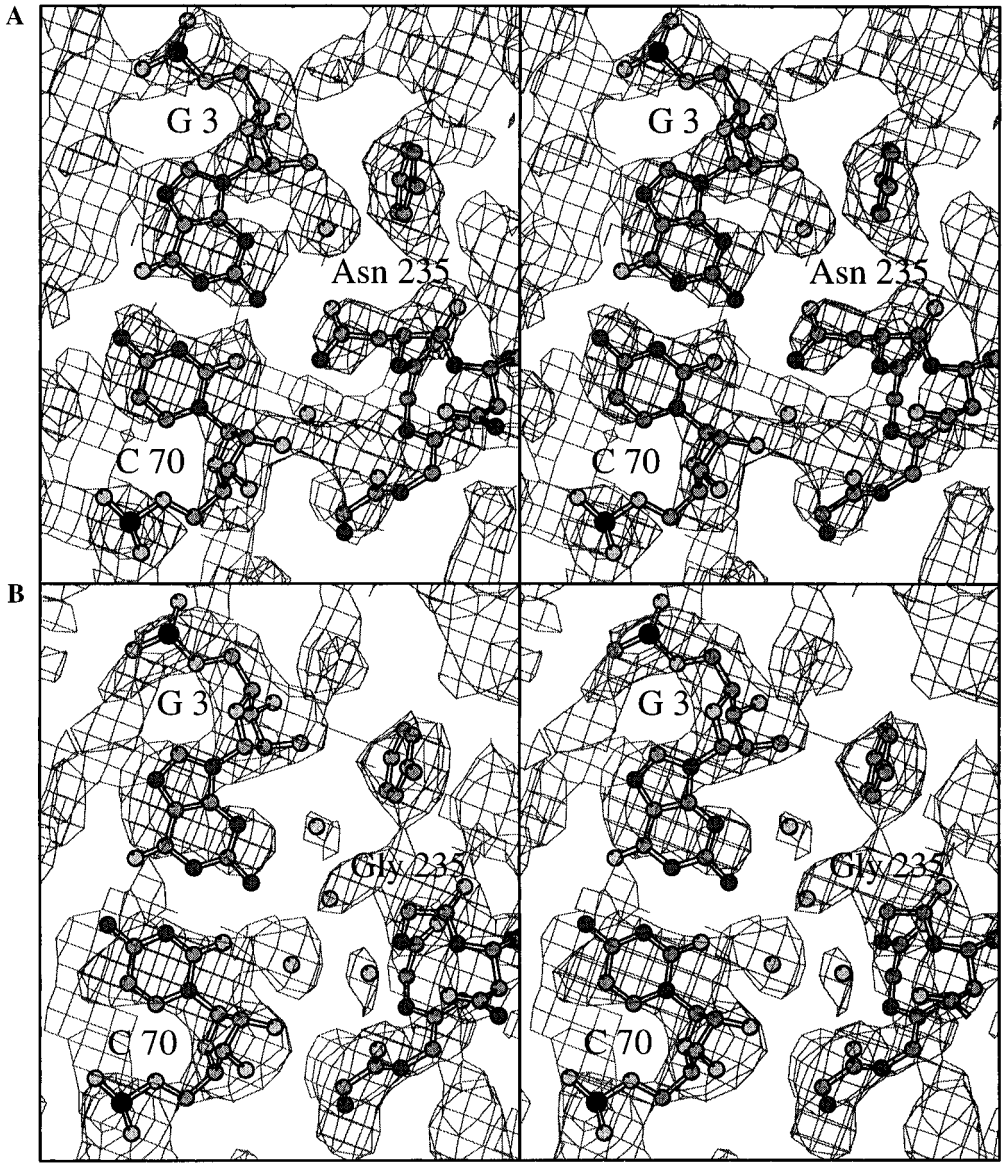

FIGURE 2: Stereoviews of the refined structures of mutant GlnRS proteins complexed with $tRNA^{Gln}$ and ATP fit into their corresponding $F_o - F_c$ simulated annealing omit maps (contoured at 0.8σ). Superposed on these maps are the backbone of helix H and residue 235 of GlnRS, base pair 3−70 of the tRNA, and associated ordered water molecules in (A) GlnRS7 and (B) GlnRS10, each complexed with $tRNA^{Gln}$. The simulated annealing omit map was computed as described in the text.

difference map was calculated using $F_o - F_c$ as coefficients. In each case, the intermediate model of the mutant complex fit the map well; only some water molecules needed to be adjusted. The fit of the final structures of GlnRS7 and GlnRS10 proteins complexed with $tRNA^{Gln}$ in the region at residue 235 in the simulated annealing omit maps is shown in Figure 2.

The initial GlnRS15 model was obtained by changing Ile129 to Thr in the final refined 4 °C wild-type structure and adjusting the resulting side chain to the F_o(mutant) − F_o(wild type) and $2F_o$(mutant) − F_o(wild-type) electron density maps. This model was then refined by imposing high harmonic restraints throughout the complex except in the 10 Å sphere surrounding Thr129. This was done since the data-to-parameter ratio is very low due to the low resolution of the data set compared to those of the wild-type and other two mutant complexes.

All structures were checked against $2F_o - F_c$ maps as well as examined using the program PROCHECK (Laskowski *et al.*, 1993) during the latter stages of the refinement. The final crystallographic *R*-factor is 20.7% for the GlnRS7 and 21.6% for the GlnRS10 complexes for all data in the resolution range 6−2.6 and 6−2.7 Å, respectively. It is 23.0% for the GlnRS15 complex for all data between 7.0 and 3.0 Å. All ϕ/ψ angles are within the allowed regions of the Ramachandran plot, with 85% or more in the most favored regions. The stereochemistry and geometry of the final structures were analyzed using the program PROCHECK and found to be better than the average of the reference structures. The root-mean-square (rms) coordinate error was estimated by the method of Luzatti (1952) to be about 0.4 Å. The final refinement parameters are summarized in Table 2. The coordinates have been deposited in the Brookhaven Protein Data Bank.

RESULTS

Difference Electron Density Maps. A difference Fourier electron density map computed using F_o(mutant) − F_o(wild type) as amplitudes and calculated phases derived from the refined structure of the wild-type complex shows that

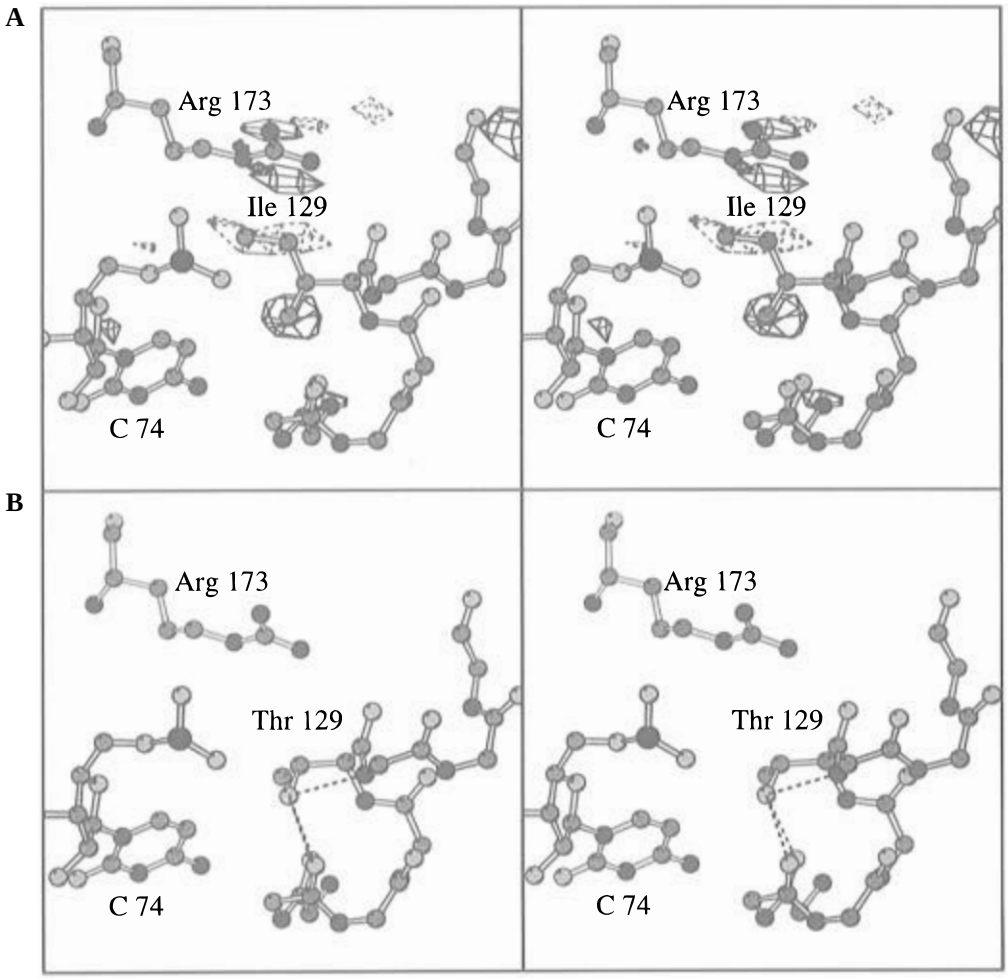

FIGURE 3: Stereoviews of (A) the region around Ile129 in the wild-type complex superposed on a F_o(GlnRS15) − F_o(GlnRS) difference electron density map contoured at 4σ, where σ = 1e/Å^3. The positive differences are drawn in black and the negative differences in dashed gray. GlnRS15 complexed with tRNA^{Gln} is structurally the same as the wild-type complex. Thr129 rotates approximately 100° about the Cα−Cβ bond. Arg173 shifts slightly toward residue 129. (B) Structure of the mutant complex. No new direct or indirect interactions with the tRNA can be found as a result of this mutation.

GlnRS15 complexed with tRNA^{Gln} and ATP undergoes very little structural change beyond the mutated residue as a result of the substitution of Ile129 with Thr. Negative difference electron density is consistent with the loss of the γ- and δ-methyl groups of Ile129 (Figure 3A). The positive difference peak in the vicinity and the lack of difference density on the β-branch methyl group suggest a rotated position of the Thr side chain (Figure 3B). These small structural shifts due to the mutation occur in the binding pocket for C74, the first C in the CCA terminus of the tRNA.

In contrast, for the GlnRS7 and GlnRS10 proteins complexed with tRNA^{Gln} and ATP, more substantial differences in electron density occur in the area surrounding residue 235 (Figure 4a,b), which is an Asn in GlnRS7, a Gly in GlnRS10, and an Asp in wild-type GlnRS. The GlnRS7 complex shows the most extensive changes in the structure, the biggest of which occur at residue 235 and its immediate vicinity on helix H (Figure 4C). Furthermore, there are changes along the backbone of the tRNA, although positions of the bases do not move very much. Changes in the protein structure are more limited in GlnRS10. The loss of the side chain in position 235 is readily apparent (Figure 4D). However, there are not many displacements even in the immediate vicinity of the residue on the helix. In the tRNA, only the backbone seems to be substantially perturbed, as in the GlnRS7 complex. In the GlnRS10 complex the stronger shifts occur at the 5′ end, while in the GlnRS7 complex the 3′ end is shifted more. Overall, the structural disruptions occur in the same general area in both complexes, and small perturbations

Table 2: Summary of Crystal Structure Refinement[a]

	GlnRS7	GlnRS10	GlnRS15
resol (Å)	6.0−2.6	6.5−2.7	7.0−3.0
n. refl	34339	32631	22183
compl (%)	91.1	95.8	90.6
R_{cryst} (%)	20.7	21.6	23.0
n. residues	604	604	604
n. solvent	113	72	14
n. atoms	5996	5951	5896
rms deviations from ideality			
protein			
bonds (Å)	0.009	0.010	0.013
angles (deg)	1.477	1.498	1.650
tRNA			
bonds (Å)	0.006	0.006	0.007
angles (deg)	1.227	1.213	1.328
ATP			
bonds (Å)	0.007	0.007	0.013
angles (deg)	1.693	1.157	1.490

[a] resol, resolution range; n. refl, number of reflections; compl, completenes of data in the given resolution shell; n. residues, number of nonsolvent residues; n. solvent, number of solvent atoms; n. atoms, total number of atoms. $R_{cryst} = (\sum_{hkl}||F_{o,hkl}| - |F_{c,hkl}||)/\sum_{hkl}|F_{o,hkl},|$.

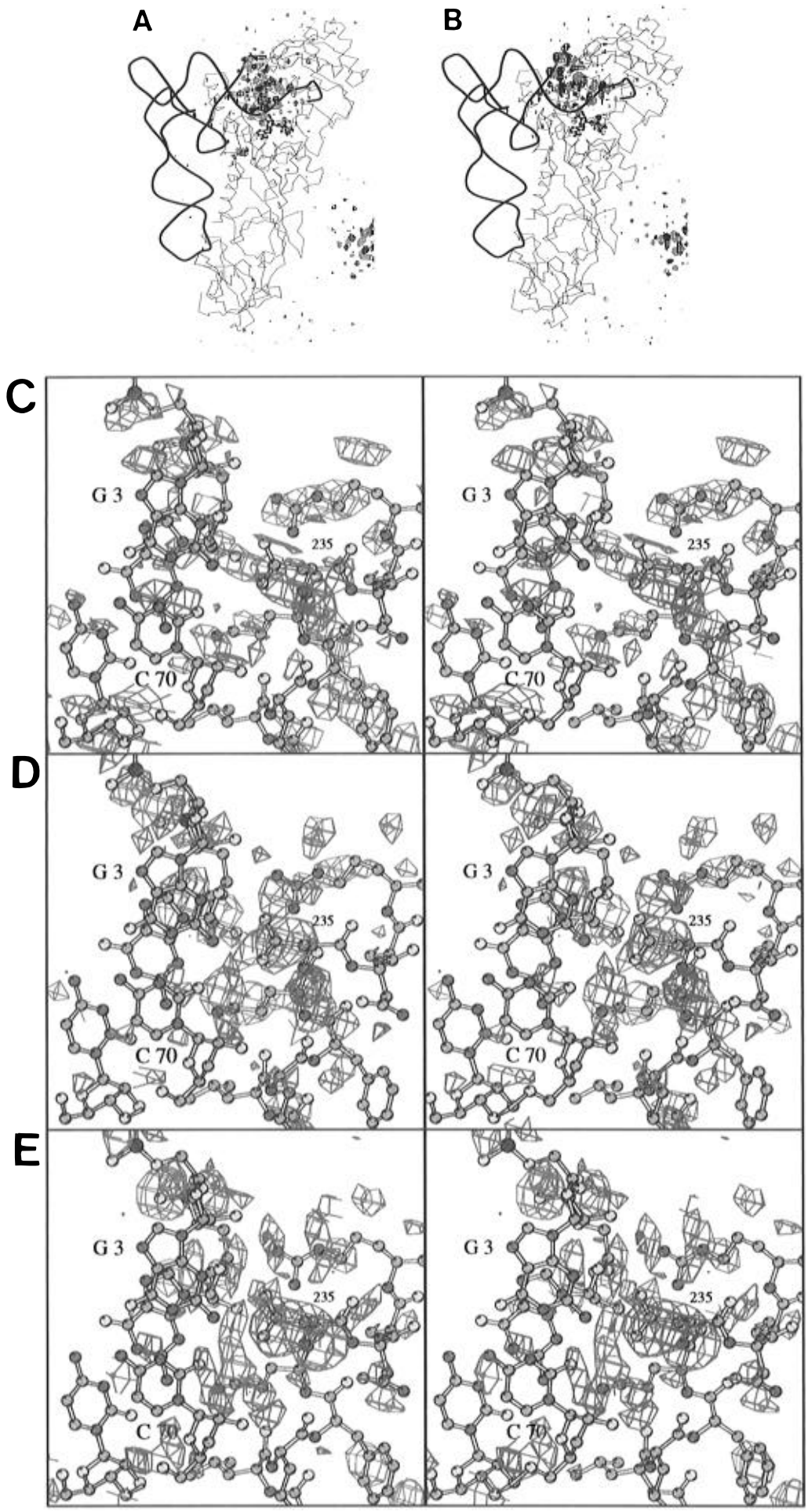
A
B
C
G 3
235
C 70
D
G 3
235
C 70
E
G 3
235
C 70

even extend to the active site. Structural changes in the two mutant GlnRS complexes are not similar, however, which is shown in a difference Fourier electron density map calculated using F_o(GlnRS7 complex) − F_o(GlnRS10 complex) as amplitudes and calculated phases as above (Figure 4E).

Analysis of GlnRS Mutant Structures. Slight changes (0.7−0.9 Å) in the *a* unit cell dimension of the mutant enzyme crystals compared to wild type led to an overall shift in each of the refined models. To make comparisons with the wild-type complex possible, the models of the mutant complexes were superposed on the model of the wild-type complex determined at −20 °C using the program O (Jones *et al.*, 1991), and the result is shown in Figure 5. After superposition, the overall root-mean-square (rms) difference for the active site domain was 0.4−0.5 Å (0.16 Å for the backbone alone) and 0.4 Å for the tRNA.

(i) Wild-Type GlnRS−tRNA^{Gln}−ATP. In the wild-type complex Asp235 forms one direct hydrogen bond via one of its carboxy oxygens with the 2-amino group of G3 and three indirect contacts through bound water molecules (Figure 6A): one water molecule contacts the ring nitrogen-3 of G3 and the 2′-OH group on the ribose moiety of residue 3, and the other contacts the 2′-OH group of residue 70 (Rould *et al.*, 1989). These interactions change in the mutant enzymes. The carbonyl group of Glu232 interacts with the guanidino group of Arg260, which in turn forms a salt bridge with the phosphates of the ATP. Arg237 and Arg238 both interact with the sugar−phosphate moiety between nucleotides G4 and G5.

(ii) GlnRS7−tRNA^{Gln}−ATP. The structural changes in GlnRS7 (D235N) complexed with tRNA^{Gln}, when compared with wild-type GlnRS, are the most extensive of the three mutant complexes. In the refined structure of the GlnRS7 complex, the overall rms displacement of the helix is 0.8 Å, due mostly to the movement of the side chains. While the rms shift in the peptide backbone of helix H is 0.25 Å, the side chain of Asn235 rotates about its Cα−Cβ bond, resulting in the amide nitrogen moving by 1.2 Å and the carbonyl oxygen by 0.9 Å compared to the corresponding coordinates of Asp235 in the wild-type complex (Figure 5). Overall, the acceptor arm of the tRNA shifts away from the protein by an rms displacement of 0.4 Å along an axis parallel to the hydrogen bonds between the 3−70 bases. The largest shift is at the phosphate of G2, which also possesses higher *B*-factors; this may be a consequence of its immediate proximity to the disordered first nucleotide. The backbone phosphates shift away from the protein by distances ranging from 0.5 to 1. Å, while the bases move by less than 0.5 Å.

Perhaps the functionally most significant change in structure is the shift of the Asn235 side chain which results in a new alignment and an additional direct hydrogen bond with base pair 3−70: the amide nitrogen of Asn235 interacts directly with the 2-keto oxygen of C70 (Figure 6B). It also interacts through a water molecule with the 2′-hydroxyl of C70. The carbonyl oxygen of Asn235 hydrogen bonds directly with the 2-amino group of G3 and indirectly, through a bound water molecule, to the ring nitrogen-3 and 2′-hydroxyl of G3, as in the wild-type complex. The side chain of Asn235 has lower *B*-factors than those of its wild-type counterpart. Thus, the structure of the mutant enzyme is locally more rigid and contains an additional hydrogen contact, which is consistent with the observed increase in binding affinity of GlnRS7 for the cognate tRNA (Hoben, 1984).

In addition, the side chain of Arg238 of helix H undergoes significant conformational changes ranging from 1.0 to 2.4 Å for atoms in the guanidino group of Arg238, although its interaction with the backbone did not change appreciably compared to the wild type. Also, the carboxylate of Glu232 moves by 0.4−1.0 Å away from the active site. No structural changes were observed in the active site.

(iii) GlnRS10−tRNA^{Gln}−ATP. The structural change in GlnRS10 (D235G) complexed with tRNA^{Gln} seen in the difference electron density map is similar in magnitude to and different in content from that found in the GlnRS7 complex. The refined model of the GlnRS10 complex shows a 0.14 Å rms change in the polypeptide backbone of helix H and only slight changes in some of its side chains, with a 0.32 Å overall rms difference from the wild-type complex. Most of the change is concentrated in the acceptor arm of the tRNA, which moves away from the protein by an rms displacement of 0.4 Å along an axis perpendicular to and in the same plane as the hydrogen bonds between the base pair 3−70 (Figure 5). As in the GlnRS7 complex, the changes are primarily in the backbone. The side chain extremity of Glu232 shifts by approximately 1 Å. As in the GlnRS7 complex, no structural changes were observed in the active site.

Again, the functionally most significant changes appear to be in the interaction between Gly235 and the G3-C70 base pair that is recognized in the wild-type enzyme. The substitition of a Gly for Asp235 removes the side chain and thus all direct and indirect contacts between the residue and base pair 3−70 (Figure 6C). The void resulting from the loss of the side chain is filled with a network of ordered water molecules. Some of the waters are within van der Waals distance from Gly235. The *B*-factors in this region are essentially the same in both GlnRS10 and wild-type GlnRS, implying similar rigidity in both cases. The two additional water molecules, compared to the wild-type complex, replace the two oxygen atoms of the wild-type Asp235. Since tRNA molecules are highly hydrated, it is possible that these water molecules are normally present in the uncomplexed tRNA and are displaced by the wild-type Asp235 but not by Gly235.

FIGURE 4: Difference electron density maps calculated using F_o(mutant) − F_o(wild type) as Fourier coefficients are superposed on the structure of the wild-type complex. Overall view of the difference density in the (A) GlnRS7 and (B) GlnRS10 complexes. The α-carbon backbone of GlnRS is traced in light gray and the tRNA in thick solid black, and the ATP is rendered in ball-and-stick representation. Each map covers the entire molecule. The density seen in the lower right quadrant is from a symmetry-related complex. The positive differences in electron density are shown in blue, and the negative differences in electron density are drawn in red. The maps are contoured at 4σ, where $\sigma = 1e/Å^3$. Detailed stereoview of the difference maps in the region around residue 235 in (C) GlnRS7 and (D) GlnRS10. Although the changes in these two complexes seem similar in scope, they are in fact different, which is shown in (E), a difference electron density map calculated with Fourier coefficients F_o(GlnRS7) − F_o(GlnRS10). Figures 2, 3, and 4 were drawn using MINIMAGE (Arnez, 1994) followed by MOLSCRIPT (Kraulis, 1991).

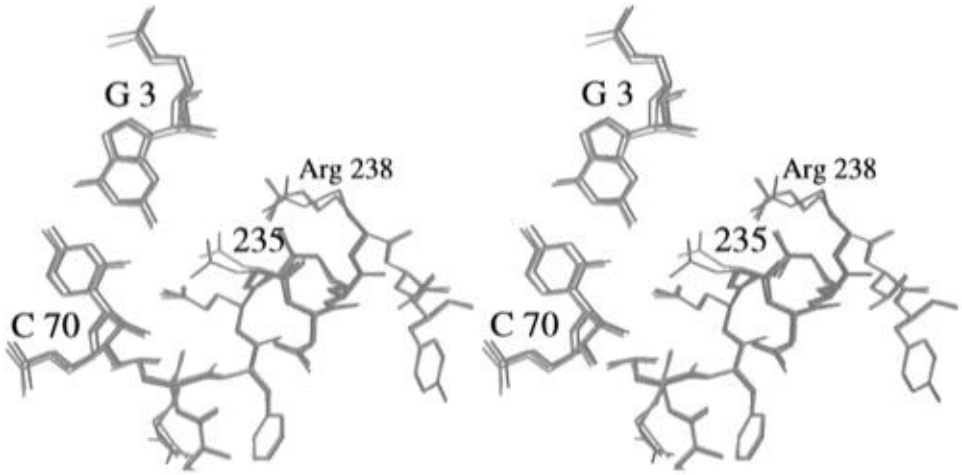

FIGURE 5: Stereoview of the superposition of the wild-type and two mutant GlnRS−tRNA^{Gln}−ATP complexes. The wild-type GlnRS complex is rendered in green, the GlnRS7 complex in blue, and the GlnRS10 complex in red. Shown is the region at residue 235: the peptide backbone of helix H and base pair 3−70.

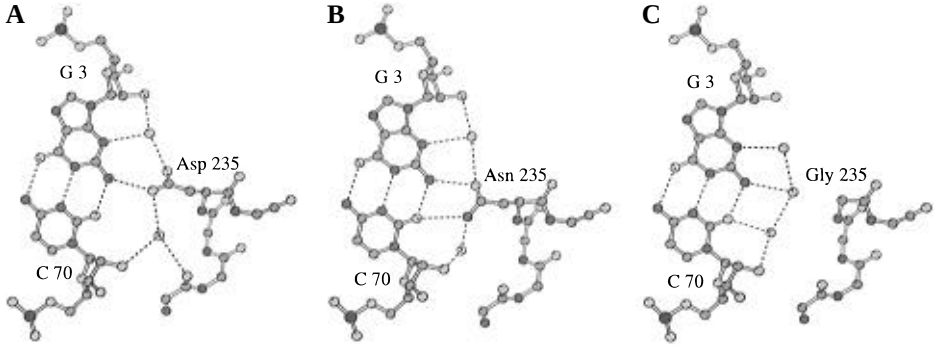

FIGURE 6: Refined structures of G3-C70 interacting with (A) wild-type GlnRS, (B) GlnRS7, and (C) GlnRS10. Asp235 forms one direct hydrogen bond with G3 and three contacts via bound water molecules. Asn235 of GlnRS7 makes two direct hydrogen bonds with G3 and C70 and two contacts with the base pair via a bound water molecule. The side chain of residue 235 has been eliminated in the GlnRS10 complex, removing all H-bond contacts between the residue and base pair 3−70.

(iv) GlnRS15−tRNA^{Gln}−ATP. The structure of GlnRS15 (I129T) complexed with tRNA^{Gln} is nearly identical to that of wild-type GlnRS−tRNA^{Gln}. The only change observed is at the site of the mutation, with a minor shift (0.1 Å) in the adjacent Arg173. The γ-oxygen of the introduced Thr129 hydrogen bonds to the peptide backbone oxygen of residue 125. Since the γ-oxygen atom is 3.8 Å away from the phosphate oxygens of C74, it cannot form direct hydrogen bonds. No additional water molecules were observed in the vicinity that would mediate such interactions (Figure 3B).

DISCUSSION

The structures of two GlnRS proteins that are mutated in residue 235 (D235N and D235G) and complexed with tRNA^{Gln} provide explanations for the lack of large changes in the mutant enzymes' charging of wild-type tRNA^{Gln} and a hypothesis for why, on the other hand, they have an increased ability to misacylate tRNA mutated in base pair 3−70. The wild-type GlnRS and mutants D235N and D235G are able to interact with wild-type base pair G3-C70 in three different ways (Figure 6). The Asn235 of GlnRS7 is able to make one additional direct hydrogen bond to G3-C70 as compared with the wild-type Asp235. Assuming that K_M is related to K_D, this extra hydrogen bond may be responsible for the decrease in K_M for tRNA^{Gln} from 0.12 mM for wild-type GlnRS to 0.014 mM for GlnRS7 (Hoben, 1984). The difference between binding free energies calculated from the K_M values by Hoben (1984) was 1.3 kcal/mol and led her to predict an additional interaction.

The complete removal of the side chain of Asp235 in GlnRS10 to give Gly235 results, of course, in no direct hydrogen bond at all with base pair G3-C70. However, a network of three H-bonded water molecules, which might be present in the uncomplexed tRNA^{Gln}, replaces the side chain of Asp235. Yet, the GlnRS10 mutant charges tRNA^{Gln} with the same kinetic parameters as wild-type GlnRS. This suggests that the enthalpic and entropic costs/benefits of replacing two tRNA-bound water molecules by the oxygens of Asp235 just balance. Our ability to accurately predict the kinetic and thermodynamic consequences of mutating either side chains or base pairs being specifically recognized is limited by the fact that two macromolecules may compensate for changes by making either alternative direct interactions or alternative interactions with water.

Since these mutant GlnRS enzymes were selected for their increased ability to mischarge *sup*F tRNA^{Tyr}, which has base pair U-A at position 3−70 rather than G-C, and since these mutant proteins nevertheless charge tRNA^{Gln} with nearly the same kinetic parameters as wild-type GlnRS, they are loss of specificity rather than change of specificity mutants. How, then, might these two mutant proteins work as well with U3-A70 as with G3-C70, whereas the wild-type protein does not? The wild-type Asp235 cannot form direct hydrogen bonds to U-A, and moreover the missing N2 in the U-A base

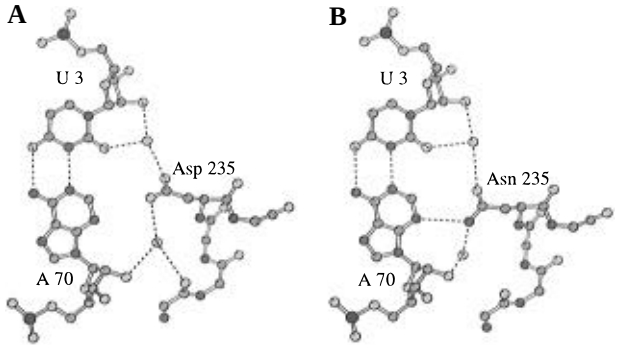

FIGURE 7: Proposed models of the interaction between base pair U3-A70 in *sup*F tRNA^{Tyr} with residue 235 in (A) wild-type GlnRS and (B) GlnRS7. To generate the model, base pair U6-A67 was copied from tRNA^{Gln} and superposed on base pair G3-C70. No changes were made in the protein structures. An Asn at position 235 can make an additional H-bond to the N3 of the adenine. Figures 1a, 5, 6, and 7 were drawn using MOLSCRIPT (Kraulis, 1991).

pair might not leave enough space for a compensating water structure (Figure 7A). Asn235 of GlnRS7 would, on the other hand, still be able to form a direct hydrogen bond with the U3-A70 base pair (Figure 7B). Presumably the same water structure can be formed with the GlnRS10 mutant whether the base pair at 3−70 is G-C or U-A, and thus Gly235 becomes a nondiscriminating mutant.

In contrast with the mutations at 235, it is not clear how the substitution of a Thr for the Ile at 129 of GlnRS15 would enhance the capacity of the mutant enzyme to misacylate *sup*F tRNA^{Tyr}. GlnRS15 has K_M and V_{max} values for tRNA^{Gln} similar to those for the wild-type enzyme and has the weakest mischarging phenotype (Swanson, 1988). The 3′ end of the tRNA molecule presumably does not play a role in tRNA discrimination by an aaRS since it is common to all tRNAs, but it may be involved in determining the V_{max} of amino-acylation. Possibly the hydrogen bonds that Thr129 forms with the backbone may strengthen the base of the helix that supports the loop whose Leu136 melts the first base pair (Rould *et al.*, 1989), which might increase the probability of melting of G1-C72 of *sup*F tRNA^{Tyr}.

The structures of the mischarging mutant GlnRS proteins complexed with tRNA^{Gln} suggest that the increased rate of misacylation results from the reduced ability of the mutant GlnRS enzymes to discriminate between cognate and non-cognate base pairs at position 3−70. To obtain more detailed insight into the misacylation phenomenon, complexes of both wild-type and these mutant proteins with tRNA molecules that are changed in base pair 3−70 need to be examined.

ACKNOWLEDGMENT

J.G.A. is grateful to Dr. M. Rould for help and guidance with data collection and other aspects of X-ray crystallography and to Dr. M. J. Rogers for discussions regarding purification of mutant GlnRS proteins. We thank Prof. D. Söll for the bacterial strains used to produce the mutant proteins.

REFERENCES

Arnez, J. G. (1994) *J. Appl. Crystallogr. 27*, 649−653.

Biou, V., Yaremchuk, A., Tukalo, M., & Cusack, S. (1994) *Science 263*, 1401−1410.

Brünger, A. T. (1990) *X-PLOR: A System for Crystallography and NMR*, Yale University, New Haven, CT.

Brünger, A. T. (1992) *X-PLOR Version 3.1. A System for X-ray Crystallography and NMR*, Yale University Press, New Haven, CT.

Delarue, M., & Moras, D. (1993) *BioEssays 15*, 1−13.

Engh, R. A., & Huber, R. (1991) *Acta Crystallogr. A47*, 392−400.

Eriani, G., Delarue, M., Poch, O., Gangloff, J., & Moras, D. (1990) *Nature 347*, 203−206.

Hayase, Y., Jahn, M., Rogers, M. J., Sylvers, L. A., Koizumi, M., Inoue, H., Ohtsuka, E., & Söll, D. (1992) *EMBO J. 11*, 4159−4165.

Hoben, P. J. (1984) Ph.D. Thesis, Yale University, New Haven, CT.

Hoben, P., & Söll, D. (1985) *Methods Enzymol. 113*, 55−59.

Hodel, A., Kim, S. H., & Brünger, A. T. (1992) *Acta Crystallogr. A48*, 851−858.

Howard, A. J., Nielsen, C., & Xuong, Ng. H. (1985) *Methods Enzymol. 114*, 452−472.

Inokuchi, H., Hoben, P., Yamao, F., Ozeki, H., & Söll, D. (1984) *Proc. Natl. Acad. Sci. U.S.A. 81*, 5076−5080.

Jahn, M., Rogers, M. J., & Söll, D. (1991) *Nature 352*, 258−260.

Jasin, M., Regan, L., & Schimmel, P. (1983) *Nature 306*, 441−447.

Jones, T. A. (1982) in *Computational Crystallography* (Sayre, D., Ed.) p 303, Clarendon Press, Oxford, U.K.

Jones, T. A., Cowan, S. W., Zou, J.-Y., & Kjeldgaard, M. (1991) *Acta Crystallogr. A47*, 110−119.

Kraulis, P. J. (1991) *J. Appl. Crystallogr. 24*, 946−950.

Laskowski, R. A., MacArthur, M. W., Moss, D. S., & Thornton, J. M. (1993) *J. Appl. Crystallogr. 26*, 283−291.

Luzatti, P. V. (1952) *Acta Crystallogr. 5*, 802−810.

Parkinson, G., Vojtechovsky, J., Clowney, L., Brünger, A. T., & Berman, H. M. (1996) *Acta Crystallogr. D52*, 57−64.

Perona, J. J. (1990) Ph.D. Thesis, Yale University, New Haven, CT.

Perona, J. J., Swanson, R., Steitz, T. A., & Söll, D. (1988) *J. Mol. Biol. 202*, 121−126.

Perona, J. J., Swanson, R. N., Rould, M. A., Steitz, T. A., & Söll, D. (1989) *Science 246*, 1152−1154.

Perona, J. J., Rould, M. A., & Steitz, T. A. (1993) *Biochemistry 32*, 8758−8771.

Rossmann, M. G., Moras, D., & Olsen, K. W. (1974) *Nature 250*, 194−199.

Rould, M. A. (1991) Ph.D. Thesis, Yale University, New Haven, CT.

Rould, M. A., Perona, J. J., Söll, D., & Steitz, T. A. (1989) *Science 246*, 1135−1142.

Rould, M. A., Perona, J. J., & Steitz, T. A. (1991) *Nature 352*, 213−218.

Ruff, M., Krishnaswamy, S., Boeglin, M., Poterszman, A., Mitschler, A., Podjarny, A., Rees, B., Thierry, J. C., & Moras, D. (1991) *Science 252*, 1682−1689.

Schulman, L. H. (1991) *Prog. Nucleic Acid Res. Mol. Biol. 41*, 23−87.

Sprinzl, M., Hartmann, T., Meissner, F., Moll, H., & Vorderwulbecke, T. (1987) *Nucleic Acids Res. 15*, r53−r188.

Swanson, R. N. (1988) Ph.D. Thesis, Yale University, New Haven, CT.

Swanson, R., Hoben, P., Sumner-Smith, M., Uemura, H., Watson, L., & Söll, D. (1988) *Science 242*, 1548−1551.

Uemura, H., Rogers, M. J., Swanson, R., Watson, L., & Söll, D. (1988) *Protein Eng. 2*, 293.

BI961532O